Check for updates

THE AMERICAN SOCIETY OF MECHANICAL ENGINEERS
345 E. 47th St., New York, N.Y. 10017

The Society shall not be responsible for statements or opinions advanced in papers or discussion at meetings of the Society or of its Divisions or Sections, or printed in its publications. Discussion is printed only if the paper is published in an ASME Journal. Authorization to photocopy material for internal or personal use under circumstance not falling within the fair use provisions of the Copyright Act is granted by ASME to libraries and other users registered with the Copyright Clearance Center (CCC) Transactional Reporting Service provided that the base fee of $0.30 per page is paid directly to the CCC, 27 Congress Street, Salem MA 01970. Requests for special permission or bulk reproduction should be addressed to the ASME Technical Publishing Department.

Copyright © 1995 by ASME All Rights Reserved Printed in U.S.A.

95-GT-102

AN EXPERIMENTAL AND NUMERICAL STUDY OF THE ISOTHERMAL FLOWFIELD BEHIND A BLUFF BODY FLAMEHOLDER

Charbel N. Raffoul and Abdollah S. Nejad
Aero Propulsion and Power Directorate
Wright-Patterson AFB, Ohio 45433

Richard D. Gould
Mechanical & Aerospace Engineering Dept.
North Carolina State University
Raleigh, North Carolina 27695

S. Alan Spring
CFD Research Corp.
Huntsville, Al 35085

ABSTRACT

An experimental and numerical investigation was conducted to study the turbulent velocities and stresses behind a 2-D bluff body. Simultaneous three-component laser Doppler velocimeter (LDV) measurements were made in the isothermal incompressible turbulent flowfield downstream of a bluff body placed at midstream in a rectangular test section. Mean velocities and Reynolds stresses were measured at various axial positions. Spanwise velocity measurements indicated that the flow is three dimensional in the recirculation zone of the bluff body. Confidence in the accuracy of the data was gained by calculating the mass fluxes at each axial station. These were found to agree with each other to within ±3%. A parallel Computational Fluid Dynamics (CFD) study was initiated to gauge the predictive accuracy of currently available CFD techniques. Three solutions were computed: a 2-D steady-state solution using the standard k-ε model, a 2-D time-accurate solution using the standard k-ε model, and a 2-D time-accurate solution using a Renormalized-Group (RNG) k-ε turbulence model. The steady-state solution matched poorly with the data, severely underpredicting the Reynolds stresses in the recirculation zone. The time-accurate solutions captured the unsteady vortex shedding from the base of the bluff body, providing a source for the higher Reynolds stresses. The RNG k-ε solution provided the best match to the data.

INTRODUCTION

Simple 2-D and 3-D bluff bodies have been the subject of experimental investigations for a number of years. Bluff-body flows exist in many places, such as the flows around flameholders in gas turbine and ramjet engines, and flows around buildings, bridges, and support structures. Some examples of recent bluff-body studies include hot-wire measurements in the flowfield behind a normal flat plate by Perry and Steiner (1987) and the work by Mansingh and Oosthuizen (1990) in the flow behind a square cylinder. Hosokawa, et al. (1993), and Geropp and Leder (1985) used a single component laser Doppler velocimetry (LDV) to document the flowfield behind a 2-D bluff body. Some researchers have found that the flowfield consists of a pair of symmetric vortices behind the bluff body with elevated turbulence levels. However, other researchers have noticed that the turbulence is created by a regular pattern of vortices shed from the trailing edge, and that the symmetric flow only exists as a time-average (Perry and Steiner, 1987; Mansingh and Oosthuizen, 1990; Raffoul, et al. 1994).

In recent years, LDV has become increasingly effective as a tool for non-intrusively measuring the instantaneous velocities at points in complex turbulent flows. Sjunnesson, et al. (1991) have used two-component LDV to study 2-D bluff bodies of various shapes, while Larousse, et al. (1991) employed two-component LDV for their study of surface mounted 3-D bodies. Few simultaneous three-component measurements have been reported to date, due mainly to the increase in instrumentation and signal processing equipment required to make the measurements. In addition, optical access is required for all three components. All of these difficulties have been overcome in the present study. Simultaneous three-component velocity measurements were made in the highly turbulent and recirculating flow past a two-dimensional bluff body. The three-orthogonal mean velocities ($\overline{U}, \overline{V}, \overline{W}$) were obtained producing profiles in the transverse and spanwise directions at 8 axial stations in the nearfield and at 11 axial stations in the farfield. All six Reynolds stresses ($\overline{uu}$, $\overline{vv}$, $\overline{ww}$, $\overline{uv}$, $\overline{uw}$, $\overline{vw}$) were also measured, as well as all triple products.

Presented at the International Gas Turbine and Aeroengine Congress & Exposition
Houston, Texas - June 5-8, 1995
This paper has been accepted for publication in the Transactions of the ASME
Discussion of it will be accepted at ASME Headquarters until September 30, 1995

Downloaded from http://asmedigitalcollection.asme.org/GT/proceedings-pdf/GT1995/78804/V003T06A016/2406276/v003t06a016-95-gt-102.pdf by guest on 21 August 2022

Like the experimental studies, many CFD researchers have conducted numerical studies on simple bluff-body geometries. These studies have produced solutions using techniques varying in sophistication from steady-state algebraic stress models Sjunnesson, et al. (1986) to the dynamic subgrid-scale Large-Eddy Simulations (LES) of Yang and Ferziger (1993). Some early solutions modeled only half of the symmetric geometry, thus imposing symmetry on the flow. However, more detailed studies have shown that the instantaneous flowfield consists of a structured pattern of alternating large scale vortices. A symmetry plane enforced by the numerical model precludes the formation of the shed vortices, relying on the turbulence model to predict any turbulent fluctuations in the wake. Comparisons to data have shown such predictions to be inadequate for bluff-body flowfields. Recently, researchers have improved the numerical modeling by including the entire flowfield. When solved with time-accurate algorithms, the flow is free to oscillate about the geometric symmetry plane. Such oscillations add significantly to both the turbulent normal and shear stresses in the wake of the bluff body. Of particular interest is the Renormalization Group (RNG) theory first applied to the k-ε turbulence model by Yakhot and Orszag (1986), and later improved by Yakhot, et al. (1992). The goal of the RNG theory is to systematically remove the smallest turbulent scales to a point where the remaining scales are resolvable. The constants used in the RNG k-ε model are derived from theory, removing much of the ad-hoc nature of the standard k-ε model, and represents the major functional difference between the models. The current study presents results from three solutions: 1) a symmetric, steady-state k-ε solution; 2) a standard k-ε, time-accurate solution; and 3) an RNG k-ε, time-accurate solution. All solutions are two dimensional, and the mean velocities and Reynolds stresses are compared to the data.

EXPERIMENTAL SETUP

Facility

A schematic of the tunnel and the 2-D test section is shown in Figure 1. The test facility is located in Test Cell 18 at the Aero Propulsion and Power Directorate of Wright Laboratory, and was specifically designed and constructed to accommodate flow visualization and laser based diagnostics. Full-view fused quartz windows on the top, bottom, and the two side walls provide optical access to the 76.2 mm x127 mm x 762 mm (3 in x 5 in x 30 in) test section. The air flow was supplied by a radial fan blower followed by a 152.4 mm (6 in) diameter honeycomb flow straightening section and settling chamber. The flow straightener was placed close to the fan outlet to minimize the large scale turbulence produced by the fan. The air was further conditioned by passing through another honeycomb flow straightener placed 304.8 mm (12 in) upstream of the test section. For the current study, the inlet centerline reference velocity (U_{ref}) was constantly monitored upstream of the bluff body at x/H = -24, using a pitot/static tube connected to a high resolution manometer. The inlet reference velocity was 23.78 m/s (78 ft/s), corresponding to a tunnel Reynolds number of $2.0x10^4$ based on inlet flow conditions and the bluff-body base height.

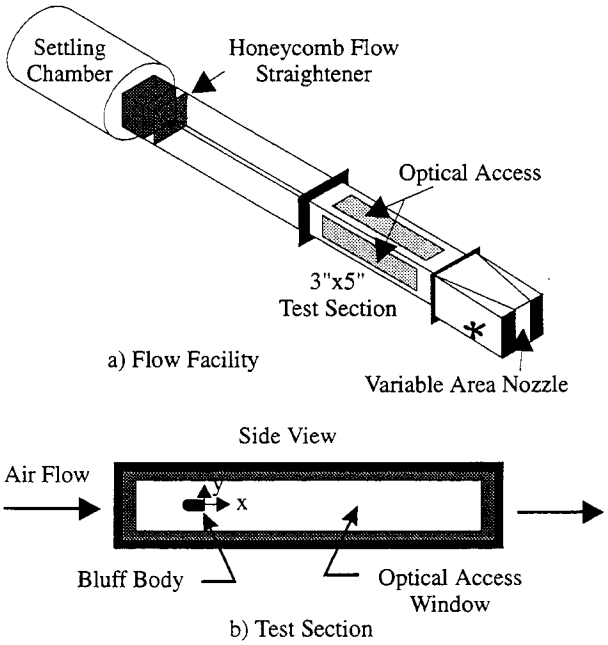

Figure 1. Experimental test facility.

Bluff Body

A schematic of the bluff-body model and its orientation to the coordinate system is shown in Figure 2. The 25.4-mm (1-in) long model consisted of: 1) a 6.35-mm (0.25-in) diameter hemispherical nose, 2) a 15.875-mm (0.625-in) long rectangular center section and, 3) a 3.175-mm (0.125-in) base/dump plate. The bluff-body height (H) was 12.7 mm (0.5 in), and spanned the entire test section giving a tunnel blockage of 16%. In order to measure the inlet flow conditions, the model was mounted four inches into the test section (downstream of the side window leading edge), directly to the side wall windows. This arrangement provided the best optical access for probing the entire flowfield surrounding the bluff body. Care was taken to align the bluff body with respect to the LDV probe volume by running the laser beam along the edge of the bluff body.

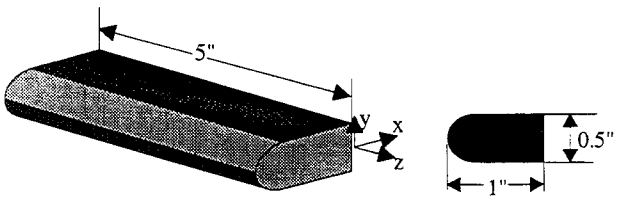

Figure 2. Bluff-body model schematic.

Downloaded from http://asmedigitalcollection.asme.org/GT/proceedings-pdf/GT1995/78804/V003T06A016/2406276/v003t06a016-95-gt-102.pdf by guest on 21 August 2022

Laser Velocimeter

A three-component LDV system operating in the forward scatter mode was mounted around the rectangular test section to make simultaneous measurements of the U, V and W-velocity components. The optical system used in these experiments involved two separate TSI Inc. laser Doppler systems. The first system used the blue (488 nm) and green (514.5 nm) wavelengths from an Argon-ion laser. These beams were conditioned and steered directly into the test section with a focal length of 300 mm. The beams passed through the side windows of the test section, allowing for the measurement of the axial and transverse (U,V) velocity components. The beams were oriented at ±45° relative to the mean flow direction, providing measurement capability very close to the base of the bluff body. For the third component, the violet laser line (476.5 nm) from another Argon-ion laser was directed via fiber-optic cable to a TSI model 9274 one-component fiber-optic probe, with a focal length of 350 mm. The violet beams were oriented orthogonal to the others, entering through the top and exiting through the bottom test section windows. Both Argon-ion lasers were operated at 1.0 Watt. To allow measurement of negative velocities, all three components were Bragg-shifted 40 MHz. The approximate probe volume dimensions were 600-μm long and 80-μm diameter for the blue and green beams and 1.5-mm long and 100-mm diameter for the violet beam. The entire system was mounted on a three-axis traversing table allowing the probe volume to be positioned to within 0.03 mm (0.001 in).

For seeding, titanium tetrachloride was introduced just downstream of the fan outlet duct, producing particles of TiO_2 less than one micron in diameter. Data rate counts of 15,000/sec/channel were routinely achieved with the TiO_2 seed. However, the coincident data rate ranged from 1000/sec in the recirculation zone to 5000/sec in the freestream and the far wake. The smooth data profiles indicated that the data rate and the applied sample size of 5120 were quite sufficient to obtain steady estimates, even for the higher moments.

Data Acquisition and Analysis

The data collection and processing system consisted of a three-channel IFA-750 Digital Burst Correlator and Analyzer by TSI, Inc. The IFA-750 allows for measurement of the Doppler frequencies of all three velocity components and has electronics to ensure that the measurements are coincident to within 20 μs. In addition to the frequency data, the time between data (TBD) and the particle residence time are recorded. All sample sets included 5120 individual velocity measurements for each velocity component. The data were filtered using a ±3 σ cut-off limit before statistical parameters were calculated. In most cases, the signal-to-noise ratio was high and very few samples were discarded. No velocity bias corrections were used in this study.

NUMERICAL TECHNIQUE

The numerical analysis for the current study was accomplished using a commercially available CFD code, CFD-ACE (Avva, 1993). CFD-ACE is a pressure based finite-volume code designed for the analysis of incompressible through hypersonic flowfields, using a modified SIMPLEC algorithm. All solutions used 2nd order accurate central differencing, stabilized with upwind biasing to solve the 2-D incompressible Navier-Stokes equations. The computational domain extended 63.5 mm (2.5 in) upstream of the bluff body (x/H = -5) and 508 mm (20 in) downstream (x/H = 40). All solutions used a constant inflow profile matched to the experimental data, and a fixed pressure exit condition.

The first solution enforced symmetry by modeling only half of the geometry. The solution was converged to steady state on a 102x38-grid (Figure 3), using the standard k-ε model with wall functions.

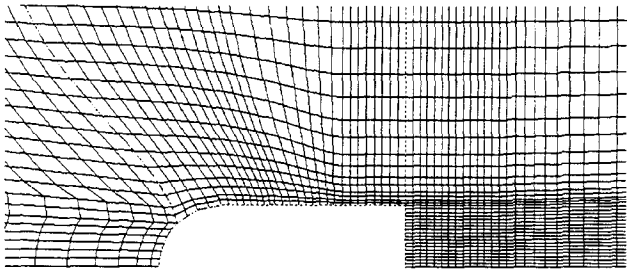

Figure 3. Grid near bluff body used for CFD analyses.

The Reynolds stresses for the steady-state solution were calculated from the Boussinesq equation;

$$\overline{u_i u_j} = \frac{\mu_t}{\rho}\left(\frac{\partial \overline{U}_i}{\partial x_j} + \frac{\partial \overline{U}_j}{\partial x_i}\right) - \frac{2}{3}k\delta_{ij} \qquad (1)$$

where; $$\mu_t = 0.09\,\rho\,\frac{k^2}{\varepsilon} \qquad (2)$$

The second solution modeled the entire flowfield on a 102x77-grid (mirror of symmetric grid) and required a time-accurate solver. Again, the standard k-ε model was used with wall functions. The solution was first advanced 200 iterations in a steady-state mode to establish the flowfield, and to allow an asymmetry to develop. The solution was then restarted in a time-accurate mode and advanced 4500 time steps at 5.0×10^{-6} sec per time step. Finally the solution was advanced ~2500 time steps to collect the turbulence statistics. Care was taken to ensure that the statistics were collected over a whole period of the vortex shedding cycle. Turbulence statistics were calculated in a fashion similar to the experimental procedure, with each time step producing one sample.

Some researchers have found that the k-ε model damped the unsteady flow behind bluff bodies (Franke, et al. 1991). However, other researchers have found the damped behavior to be a function of the differencing scheme and not the turbulence model (Przuli, et al. 1993). In the current study, the k-ε model converged to a steady state with first order differencing, but properly predicted the vortex shedding with central differencing.

Downloaded from http://asmedigitalcollection.asme.org/GT/proceedings-pdf/GT1995/78804/V003T06A016/2406276/v003t06a016-95-gt-102.pdf by guest on 21 August 2022

The third solution was completed in a similar manner except the RNG k-ε model was employed. One of the major differences between the standard k-ε model and the RNG k-ε model, is that many of the constants are derived from the RNG theory, removing much of the ad-hoc nature of the standard k-ε model. For comparison, the standard k-ε constants used in the current study are as follows: $C_\mu = 0.09$, $C_{\varepsilon 1} = 1.44$, $C_{\varepsilon 2} = 1.92$, $\sigma_\kappa = 1.0$, and $\sigma_\varepsilon = 1.3$.

In contrast, the RNG theory derives the following constants; $C_\mu = 0.085$, $C_{\varepsilon 2} = 1.68$, $\sigma_\kappa = 0.7179$, and $\sigma_\varepsilon = 0.7179$.

$$C_{\varepsilon 1} = 1.42 - \frac{\eta\left(1-\frac{\eta}{\eta_o}\right)}{1+\beta\,\eta^3} \qquad (3)$$

where; $\eta = Sk/\varepsilon$, $S = \sqrt{2S_{ij}S_{ij}}$, $\eta_o = 4.38$, and $\beta = 0.015$.

Note that C_{ε_1} is no longer a constant. Using the new constants, the RNG k-ε model was found by Speziale and Thangam (1992) to give excellent results for the backward-facing step flow of Kim, et al. (1978). The reader is referred to Yakhot, et al. (1992) for more information on the RNG theory.

EXPERIMENTAL RESULTS AND DISCUSSION

Mean Velocity Data

Measurements of the normalized mean axial velocity and the normalized fluctuating axial velocity are shown in Figures 4 and 5, respectively. All measurements are normalized with respect to the reference velocity, $U_{ref} = 23.78$ m/s (78 ft/s), and the bluff-body height, H = 12.7 mm (0.5 in). At first, single component velocity measurements were made using the green laser beam which allowed measurements to be made from top to bottom walls. Such detailed measurements of the mean axial velocity allowed for the calculation of the mass flow rates at each axial station. These were found to be within ±3% of each other throughout the flowfield. Three-component measurements gave virtually identical results (Raffoul, et al. 1994). The bluff-body dump plane (i.e., the trailing edge) is assigned the axial position x = 0, with negative x values referring to measurement stations upstream of the bluff body. Figure 4 shows that the inlet flow is very symmetric and uniform. At the downstream stations, the presence of the wake from the bluff body can be clearly seen in the center of the flow, as well as the presence of two shear layers. The recirculation zone behind the bluff body is roughly one bluff-body thickness in length, significantly smaller than the recirculation region behind a backward-facing step which is known to be 7 to 8 step-heights Negative axial velocities were found for x/H < 1 as shown in Figure 8. The magnitude of the reverse flow is high which results in a rather intense vortex role-up. Figure 5 shows the double hump behavior expected due to the presence of the shear layers near the top and bottom of the bluff body.

Figures 6 and 7 show the normalized transverse mean and fluctuating velocities. Due to optical access restrictions, these measurements do not extend to the top and bottom walls. Figure 6 shows that the mean transverse velocity profile at x/H = 1 is anti-symmetric as expected, since the transverse velocity is directed towards the centerline at this location. Comparison of the peak axial and transverse fluctuating velocities show that the transverse values are more than double the axial values. The velocity data were time-averaged over a 2-3 second interval for the statistics calculations. Raffoul, et al. (1994) showed that the present configuration produces unsteady flow as periodic vortex pairs are shed from the back face. Transformation of the velocity-time data for a point on the centerline of the wake at (x/H = 1) revealed a dominant frequency of $f = 454$ Hz, with a corresponding Strouhal number, St = 0.243, where;

$$St = f\,H/\,U_{ref} \qquad (4)$$

Figures 8, 9, and 10 show the evolution of the normalized mean axial, transverse, and spanwise velocities and velocity gradient distributions in the near wake, at eight axial stations. The experimental data is represented by circular symbols. The

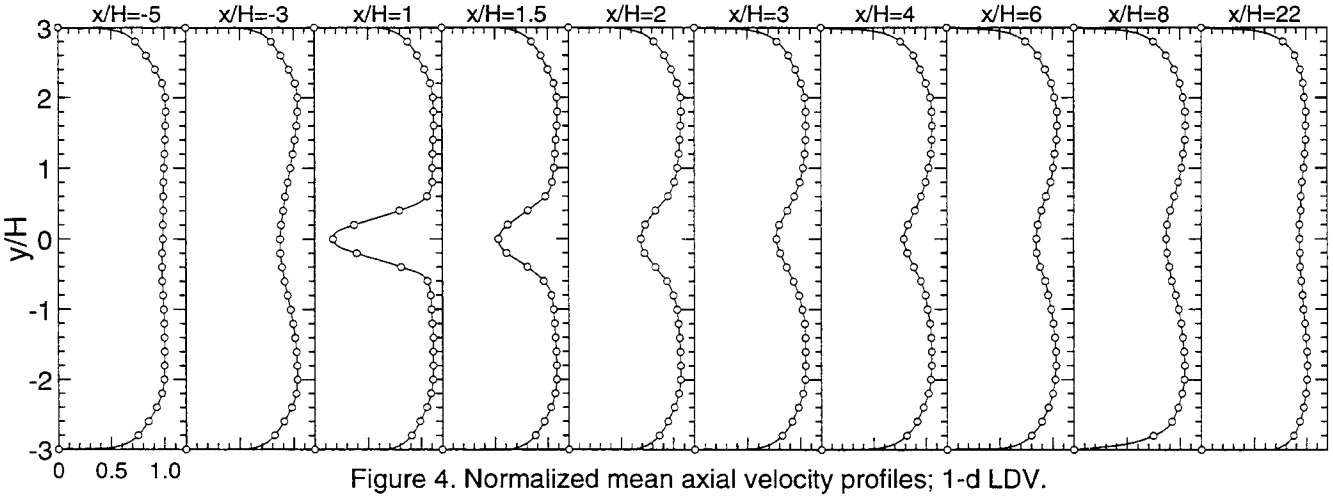

Figure 4. Normalized mean axial velocity profiles; 1-d LDV.

Downloaded from http://asmedigitalcollection.asme.org/GT/proceedings-pdf/GT1995/78804/V003T06A016/2406276/v003t06a016-95-gt-102.pdf by guest on 21 August 2022

continuous lines in figures 8, 9, and 11 through 13 represent the numerical predictions and will be discussed later. Figure 8 depicts negative velocities in the recirculation zone up to x/H = 0.9. The velocity gradients in the x- and y- directions are computed using a central difference smoothing algorithm developed by Gould (1994). The first station, located one-half bluff-body height downstream, shows a maximum velocity deficit of -0.5. The normalized y-derivative shows a maximum and a minimum at an absolute value of 4.0 while the normalized x-derivative shows a maximum of -1.0. Figure 9 shows approximately equal maximum and minimum transverse velocities (V) for all the stations. The normalized y-derivatives of the V-velocity have a minimum of -2.0 except for x/H = 0.5 and 0.6. The normalized x-derivatives of the V-velocity are relatively small, but exhibit a unique feature in that they change slope at the recirculation bubble location, where the gradient is nearly non-existent. Figure 10 shows the three-dimensionality of the flow in the wake. The continuous lines in Figures 10 and 14 represent the smoothed curve-fitted data. The spanwise component (W) peaks at nearly 10% of the freestream velocity at the first station and decreases in magnitude with downstream locations. The normalized y-derivative of the W-velocity has a maximum absolute value of about 0.4, while the normalized x-derivative of the W-velocity has a small deficit that was roughly comparable to the error band.

Turbulent Normal and Shear Stresses

Figures 12, 13, and 14 show profiles of the three measured normalized turbulent normal stresses ($\overline{uu},\overline{vv},\overline{ww}$). Peak values of the axial normalized turbulent intensity (i.e., the square root of the turbulent normal stress) occur at x/H = 1, in the shear layer, and reach a value of 31% of the freestream velocity. This value is slightly above that obtained behind of a backward-facing step (25%), as reported by Gould, et al. (1988). It is noteworthy that the peak transverse normalized turbulence intensity is 77%, approximately 2.5 times the value of the peak axial normalized turbulence intensity. The axial, transverse and spanwise turbulent normal stresses are clearly different in value and profile shapes. The different shapes indicate that the structure of turbulence in and near the recirculation zone is quite anisotropic, and remains so until x/H ≅ 8. The anisotropy implies the existence of multiple length scales in the turbulence structure. The y-derivatives of the transverse normal stress are the only significant derivatives of the normal stresses. The derivatives reach a maximum normalized absolute value of 1.5 at the first station and diminish to a value of 1.0 at x/H = 1.2. The normalized turbulent shear stresses ($\overline{uv},\overline{uw},\overline{vw}$) have also been obtained. These measurements indicate that the $\overline{uv}$ shear stress (Figure 10) is the only significant one of the three, thus the only one presented. The values of $\overline{uv}$ were found to be small at x/H = 0.5, growing to a peak value of 0.1 at x/H = 0.9, the free stagnation point. The normalized y-derivatives of $\overline{uv}$ had a minimum of -1.0 at x/H = 0.9, while the x-derivatives did not show any appreciable value.

NUMERICAL RESULTS AND DISCUSSION

Three solutions were computed as part of the current study. First a steady-state solution utilizing a symmetry plane was obtained. A time-accurate solution was then completed using the standard k-ε turbulence model. Finally, another time-accurate solution was completed using an RNG k-ε turbulence model to capture the subgrid turbulence.

The velocities and Reynolds stresses for the steady-state solution are shown with the experimental measurements in Figures 8, 9, and 11 through 13. The velocities indicate that the numerical recirculation bubble extends to x/H = 2, much further downstream than the experimental bubble. The numerical prediction has a bubble length of four step heights, similar to a backward-facing step. This is to be expected since the model resembles a backward-facing step with a slip wall at the centerline. The Reynolds stresses are also comparable to those of a backward-facing step. However, the experimentally measured Reynolds stresses for the bluff-body flow are typically 5 times higher than those found in a backward-facing step flow. The underprediction of the Reynolds stresses by the steady-state solution leads to the incorrect bubble length in the recirculation zone. For the purpose of fuel injection and mixing studies, such an analysis is not sufficient.

The time-accurate solutions were able to predict the vortex shedding behind the bluff body. The standard k-ε solution predicted a Strouhal number, St = 0.240, which compared well to the experimental value of 0.243. The time-averaged velocities and Reynolds stresses are also shown in Figures 8, 9, and 11 through 13. The separation bubble calculated with this method is considerably shorter than that predicted using the steady-state solution method, extending to x/H = 1.0. However, the bubble is still longer than what the measurements indicate, and the predicted wake spreads slightly faster than the experimental wake. While the magnitudes of the Reynolds stresses are higher than those predicted using the steady-state method, they are still lower than the experimental results.

To improve the time-accurate results, the RNG k-ε turbulence model developed by Yakhot, et al. (1992) was tested. The Strouhal number predicted by the RNG model was 0.253, slightly higher than that obtained from the experimental data. However, the mean velocity predictions were significantly improved, as shown in Figures 8 and 9. The separation bubble has shortened and now ends slightly ahead of the experimental measurements (x/H = 0.7). The overall mean velocity field is predicted fairly well, except for the transverse velocity just downstream of the reattachment point. The discrepancy of the transverse velocities may be a result of the 3-D effects near the bluff body. The spanwise velocities observed in the experiments are most likely due to the interaction of the tunnel wall boundary layers with the bluff-body flowfield; they are also probably symmetrical about the spanwise centerline. If so, the vortices shed from the bluff body will experience some degree of vortex stretching in the near-field wake. Such vortex stretching could amplify the transverse velocities.

Downloaded from http://asmedigitalcollection.asme.org/GT/proceedings-pdf/GT1995/78804/V003T06A016/2406276/v003t06a016-95-gt-102.pdf by guest on 21 August 2022

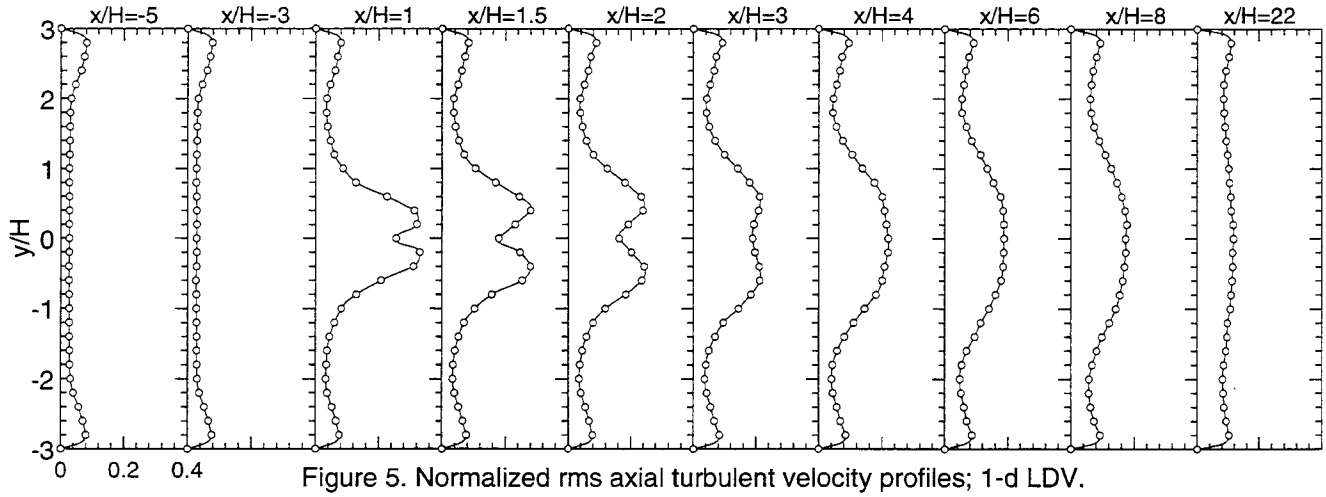

Figure 5. Normalized rms axial turbulent velocity profiles; 1-d LDV.

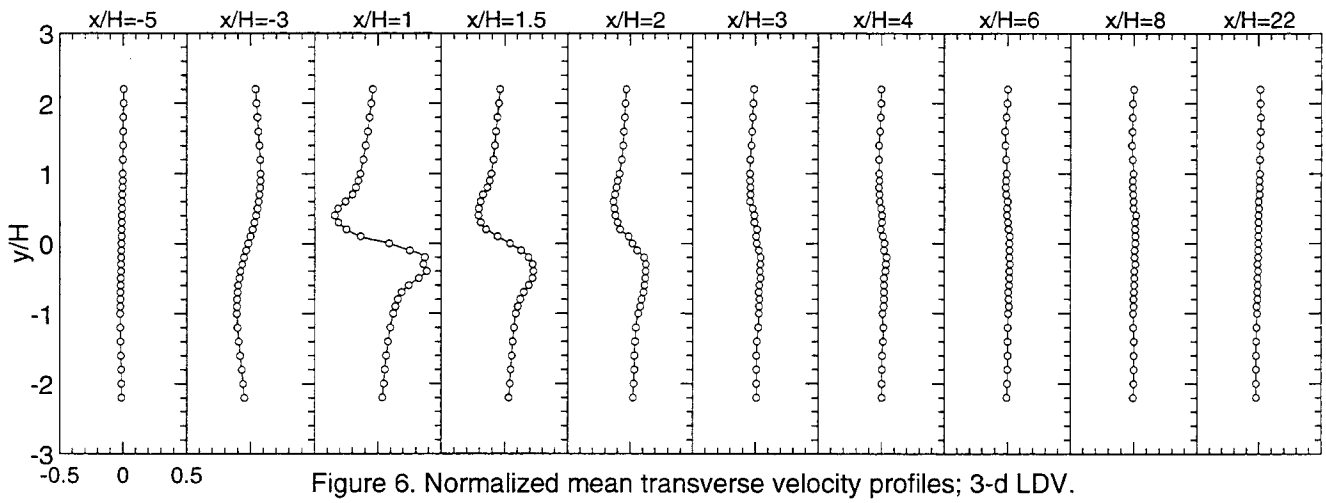

Figure 6. Normalized mean transverse velocity profiles; 3-d LDV.

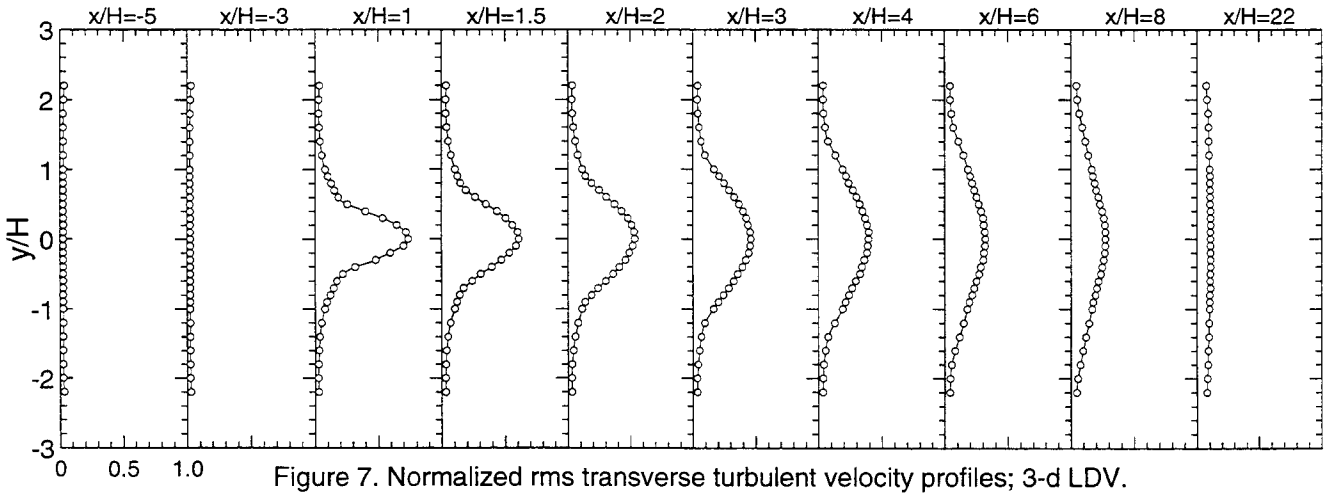

Figure 7. Normalized rms transverse turbulent velocity profiles; 3-d LDV.

Downloaded from http://asmedigitalcollection.asme.org/GT/proceedings-pdf/GT1995/78804/V003T06A016/2406276/v003t06a016-95-gt-102.pdf by guest on 21 August 2022

The comparisons of the Reynolds stresses to the measurements are improved. However, the normal stresses are overpredicted, leading to the shorter separation bubble. The largest discrepancy occurs with the transverse normal stress, the values of which are overpredicted by a factor of three. Martensson, et al. (1991) obtained similar results using LES, and found that the transverse normal stress was reduced significantly when simulated with a 3-D analysis. A 3-D solution can be expected to produce lower Reynolds stresses due to the 3-D filament distortion of the shed vortices. The 2-D vortex filament makes no contribution to the spanwise stresses. However, if the filament is allowed to distort in the spanwise direction, the vortex will make a contribution to the spanwise stresses, dependant upon the magnitude of the local distortion. Any contribution to the spanwise stresses will result in a likewise decrease in the transverse and axial stresses, dependent upon the direction of the local distortion. The proper prediction of the vortex filament distortion may be sensitive to the spanwise extent of the computational domain and may require the entire spanwise domain to be included. A 3-D analysis was attempted in the present study, using a spanwise domain of 1 base-height and periodic boundary conditions. However, the results degraded significantly. Arnal and Friedrich (1991) report that 3-D solutions of a backward-facing step with a spanwise extent less than 4 step heights can give erroneous results. A 3-D solution with a larger spanwise extent for the current geometry is under investigation.

CONCLUSIONS

Simultaneous three-component LDV measurements have been completed on a two-dimensional bluff body. The measurements revealed that the flowfield was dominated by strong, periodic vortex shedding in the wake, yielding a symmetric vortex pair in the mean flow. The mean spanwise velocity component was measured in the wake. Significant spanwise flow was found at axial stations less than x/H = 1.2, however the source for this spanwise component has not been clearly identified. The mean flow recirculation bubble behind the bluff body ended at x/H = 0.9, significantly shorter than the recirculation zone found in a backward-facing step flow. The dominant vortex-shedding frequency was found to be 454 Hz. The Reynolds stress terms involving the axial (U), and transverse (V) velocity components were of the same order of magnitude directly behind the bluff body, while those involving the spanwise (W) velocity component were negligible. Beyond the recirculation zone only the contributions involving the transverse velocity were significant.

The numerical simulations showed that the bluff-body flowfield cannot be accurately predicted using a steady-state calculation, because no mechanism exists to predict the amplified time-averaged Reynolds stresses which result due to vortex shedding. The time-accurate standard k-ε model predicts the vortex-shedding frequency accurately, but underpredicts the Reynolds stresses and overpredicts the length of the recirculation bubble by 20%. The RNG k-ε model predicts a higher vortex-shedding frequency, but obtains the closest match to the mean velocities. However, the Reynolds stresses tended to be overpredicted. A 3-D calculation covering the entire spanwise domain should improve the results.

ACKNOWLEDGMENTS

This work was performed at Wright Laboratory, Aero Propulsion and Power Directorate, Wright-Patterson Air Force Base, Ohio. Special thanks goes to the Air Force Office of Scientific Research and to Dr. Julian Tishkoff for providing sponsorship. The authors would also like to thank Mr. Cliff Smith and Dr. Andy Leonard of CFD Research Corporation for their assistance with the numerical effort.

Downloaded from http://asmedigitalcollection.asme.org/GT/proceedings-pdf/GT1995/78804/V003T06A016/2406276/v003t06a016-95-gt-102.pdf by guest on 21 August 2022

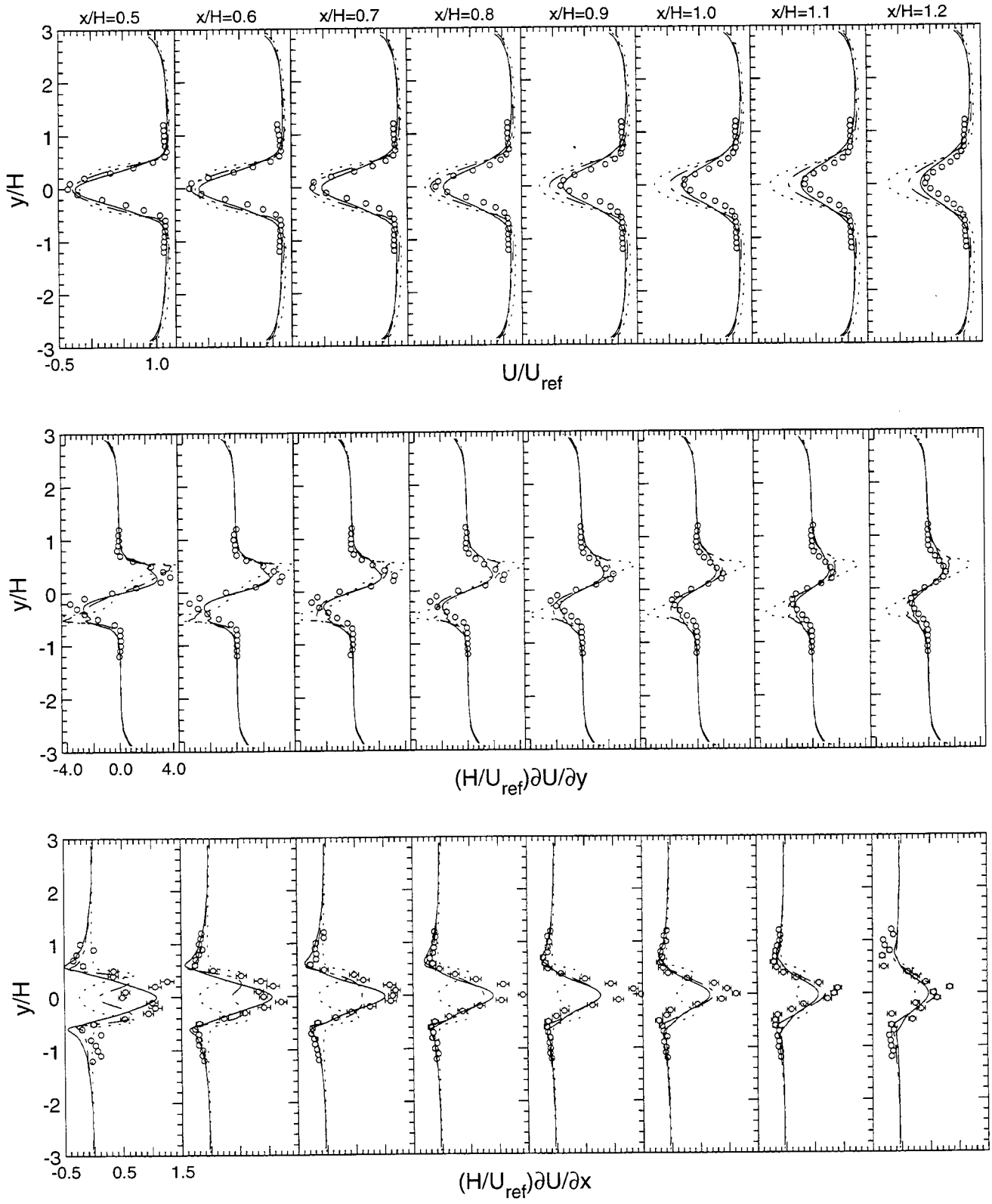

Figure 8. Normalized mean axial velocity and velocity gradient distributions
(○ data, · · · · steady state k-ε, — - unsteady k-ε, —— unsteady RNG).

Downloaded from http://asmedigitalcollection.asme.org/GT/proceedings-pdf/GT1995/78804/V003T06A016/2406276/v003t06a016-95-gt-102.pdf by guest on 21 August 2022

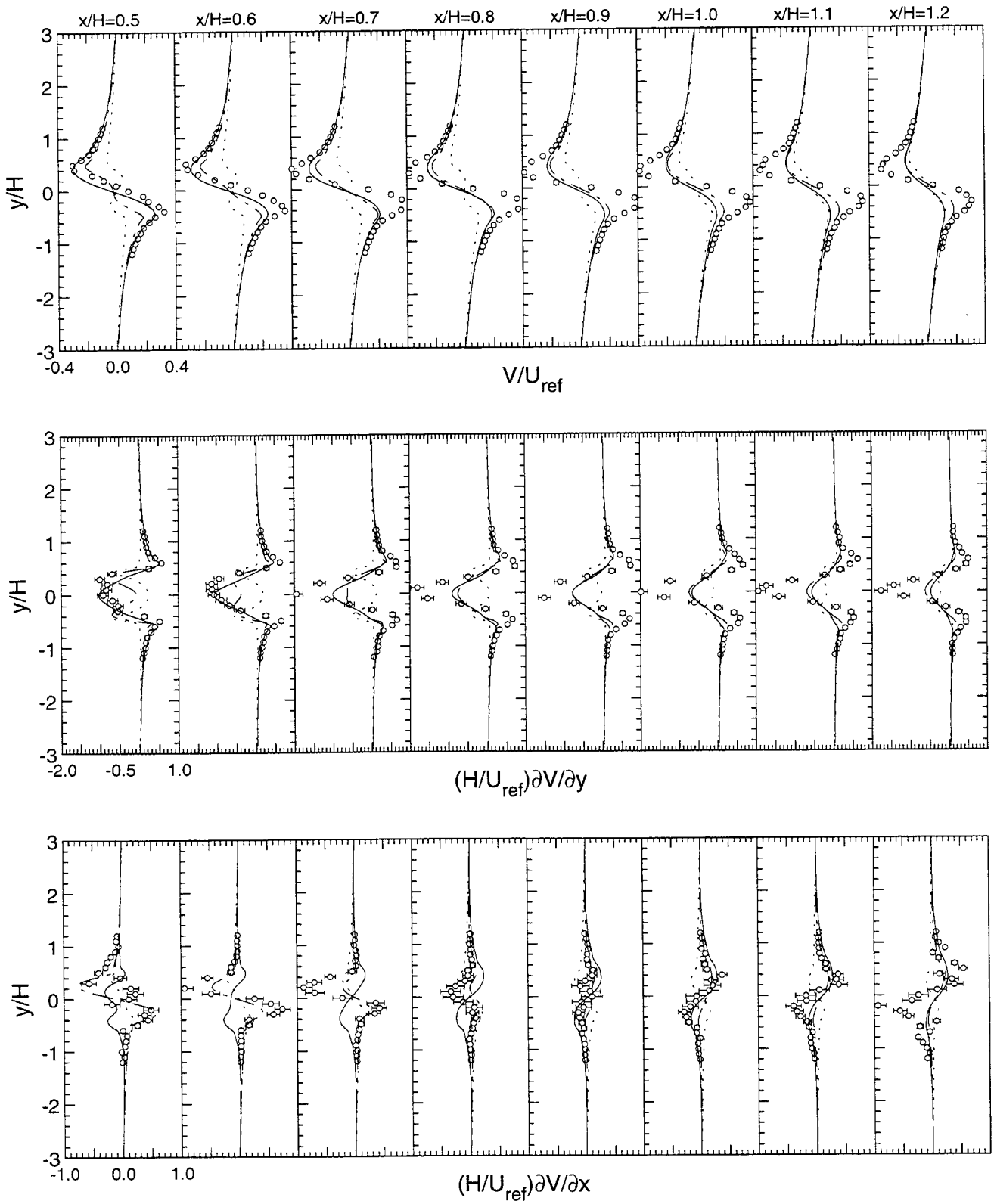

Figure 9. Normalized mean transverse velocity and velocity gradient distributions
(○ data, · · · · steady state k-ε, — - unsteady k-ε, —— unsteady RNG).

Downloaded from http://asmedigitalcollection.asme.org/GT/proceedings-pdf/GT1995/78804/V003T06A016/2406276/v003t06a016-95-gt-102.pdf by guest on 21 August 2022

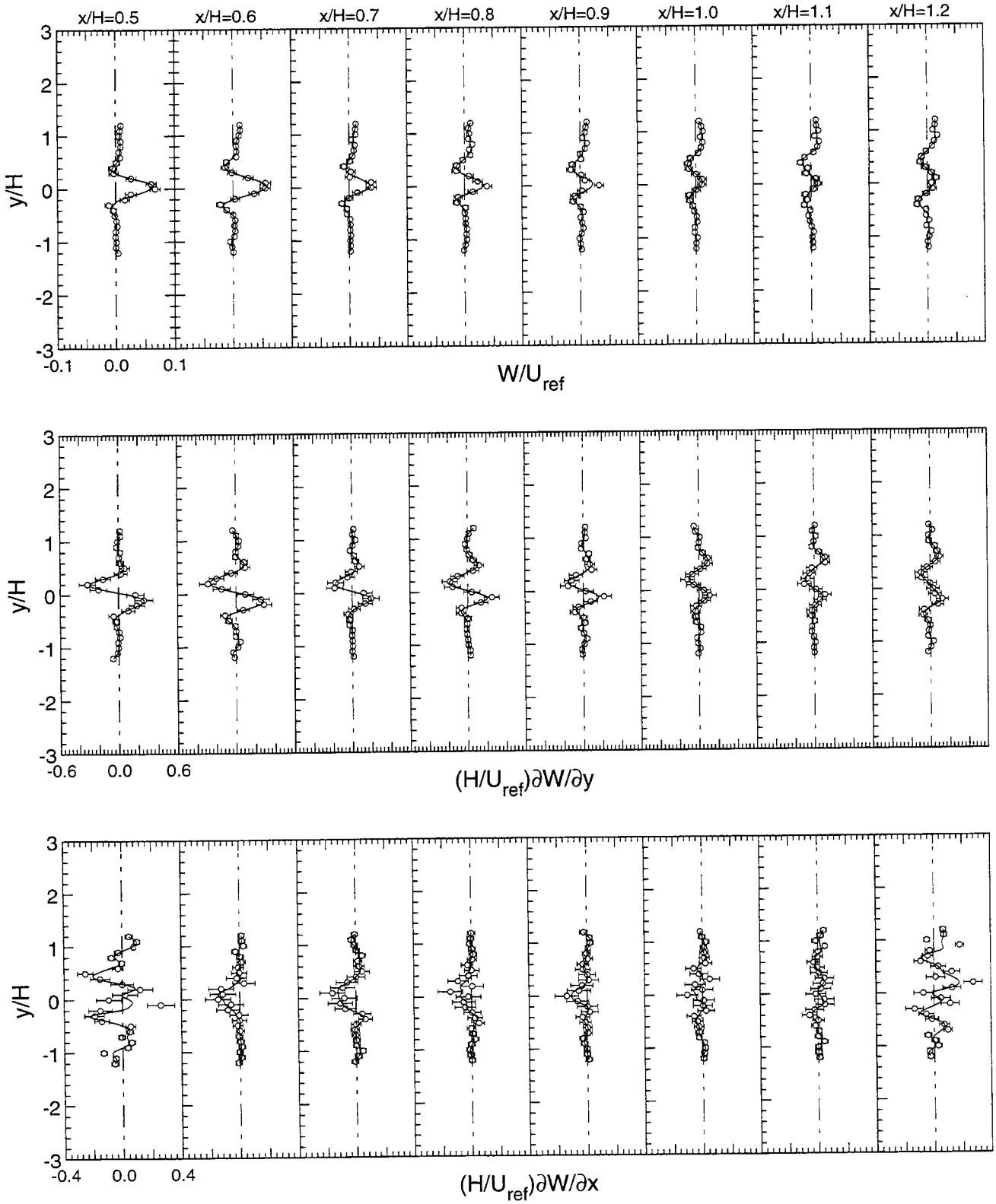

Figure 10. Normalized mean spanwise velocity and velocity gradient distributions (○ data, —— smoothed curve-fit).

Downloaded from http://asmedigitalcollection.asme.org/GT/proceedings-pdf/GT1995/78804/V003T06A016/2406276/v003t06a016-95-gt-102.pdf by guest on 21 August 2022

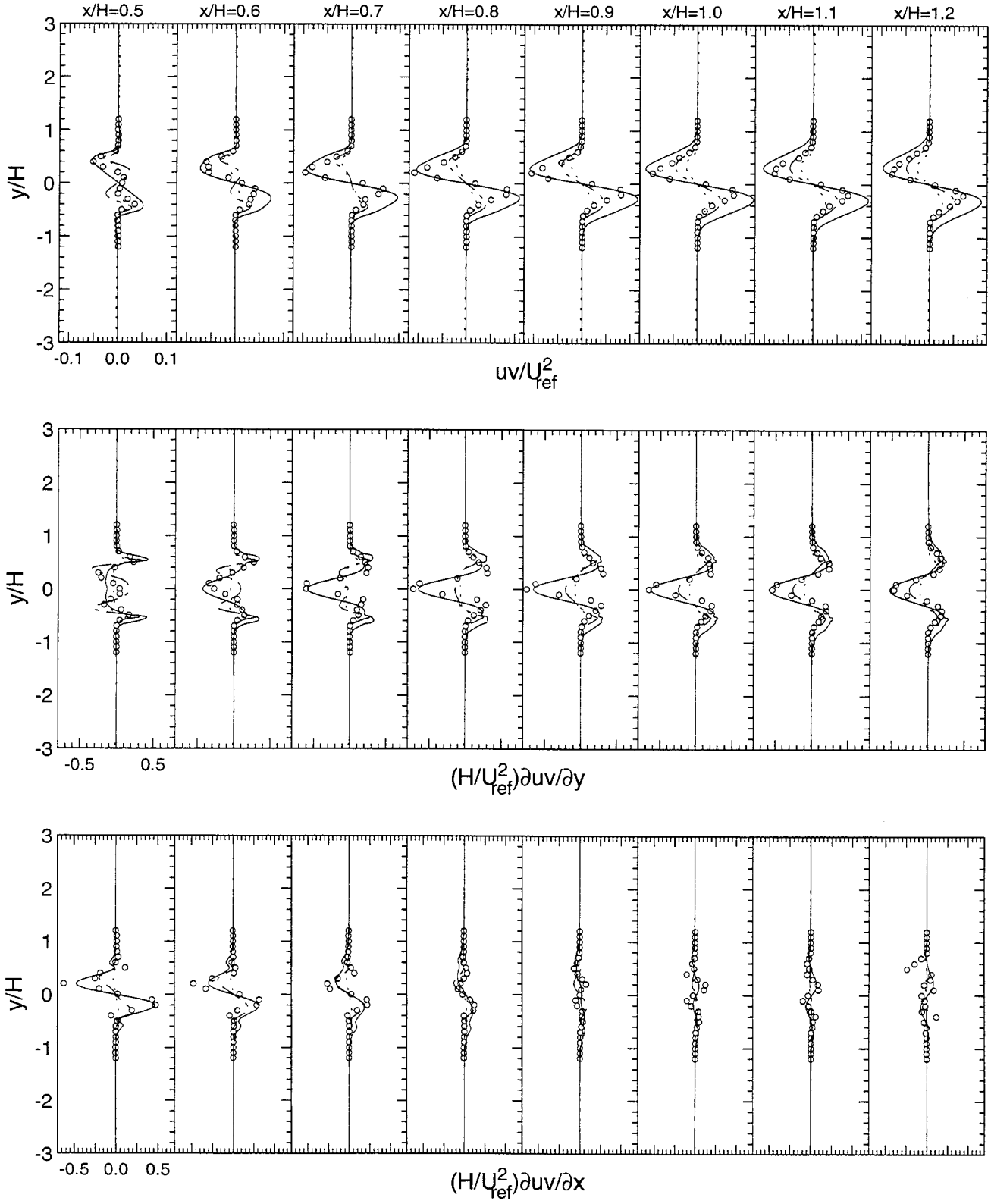

Figure 11. Normalized uv turbulent stress and stress gradient distributions
(○ data, · · · · steady state k-ε, — - unsteady k-ε, —— unsteady RNG).

Downloaded from http://asmedigitalcollection.asme.org/GT/proceedings-pdf/GT1995/78804/V003T06A016/2406276/v003t06a016-95-gt-102.pdf by guest on 21 August 2022

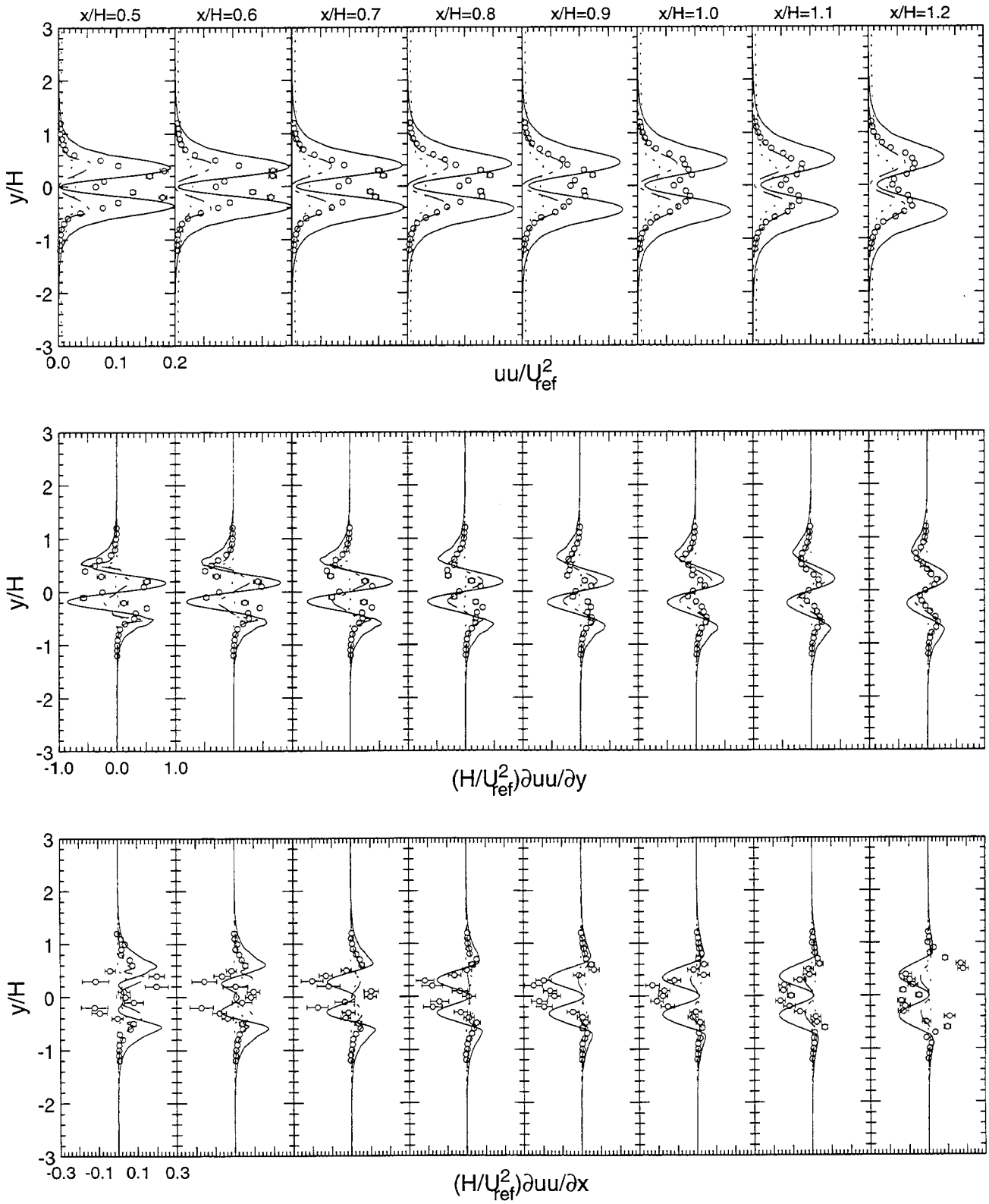

Figure 12. Normalized uu turbulent stress and stress gradient distributions
(○ data, · · · · steady state k-ε, — · unsteady k-ε, —— unsteady RNG).

Downloaded from http://asmedigitalcollection.asme.org/GT/proceedings-pdf/GT1995/78804/V003T06A016/2406276/v003t06a016-95-gt-102.pdf by guest on 21 August 2022

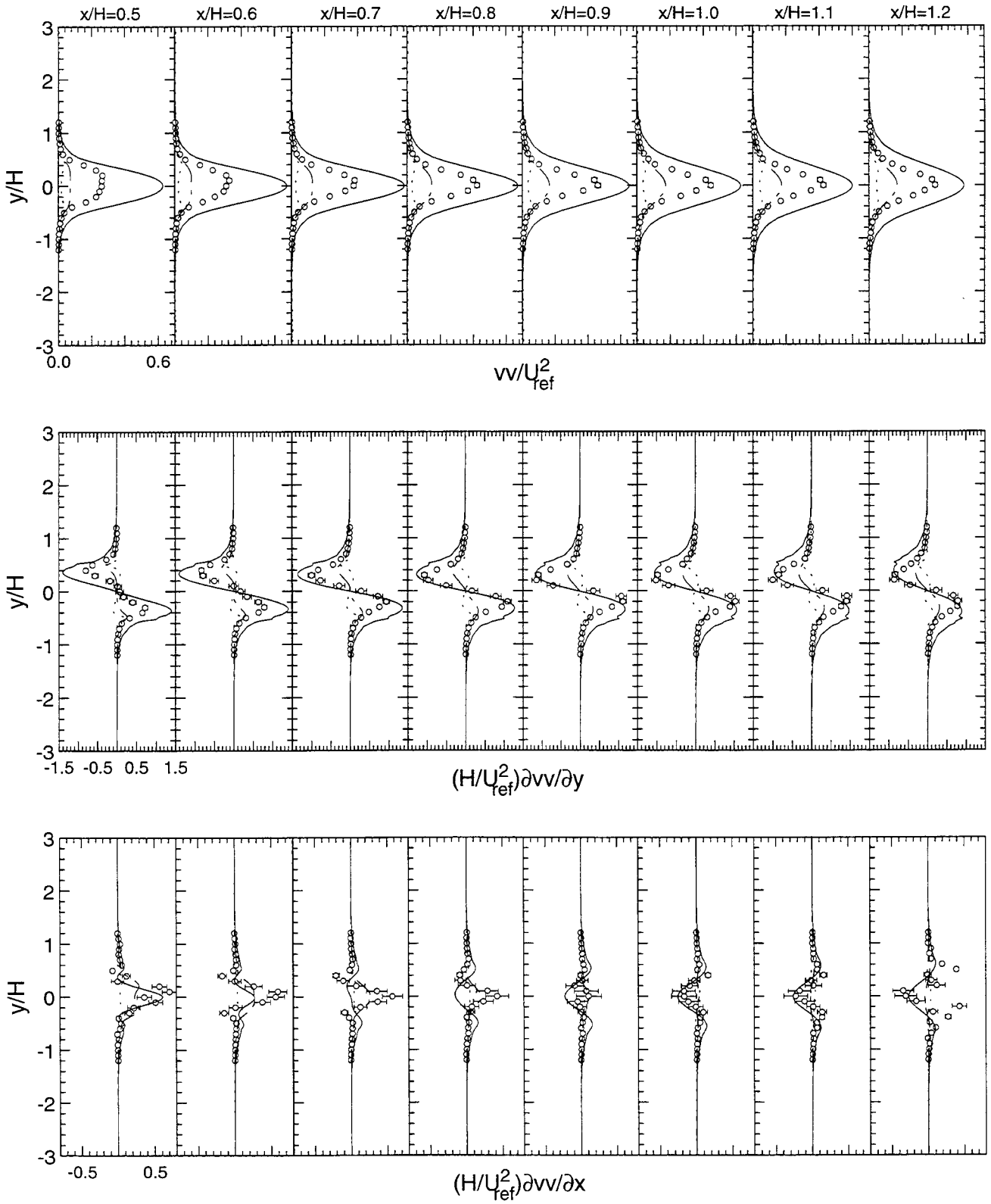

Figure 13. Normalized vv turbulent stress and stress gradient distributions
(○ data, · · · · steady state k-ε, — - unsteady k-ε, —— unsteady RNG).

Downloaded from http://asmedigitalcollection.asme.org/GT/proceedings-pdf/GT1995/78804/V003T06A016/2406276/v003t06a016-95-gt-102.pdf by guest on 21 August 2022

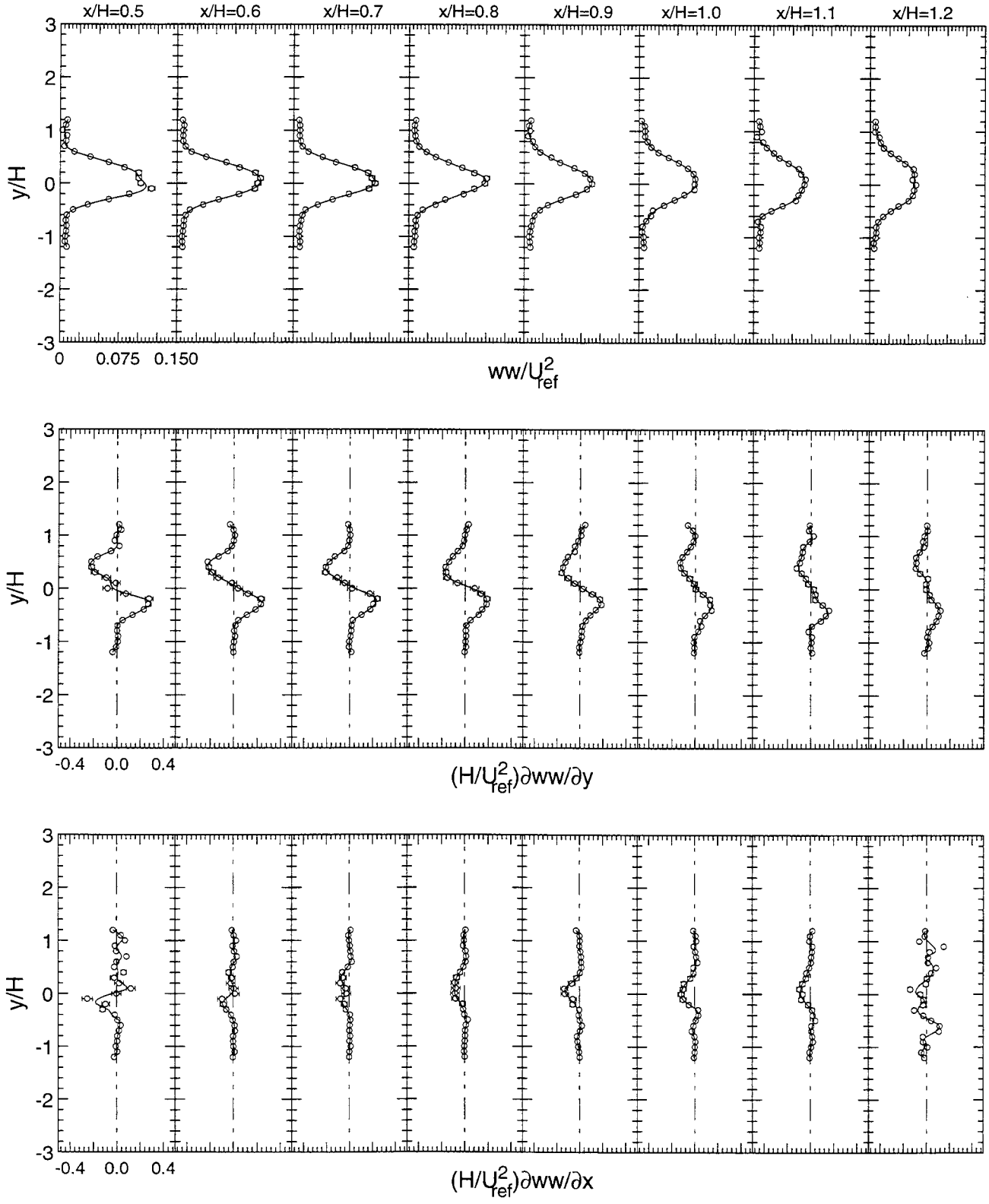

Figure 14. Normalized ww turbulent stress and stress gradient distributions
(○data, —— smoothed curve-fit).

Downloaded from http://asmedigitalcollection.asme.org/GT/proceedings-pdf/GT1995/78804/V003T06A016/2406276/v003t06a016-95-gt-102.pdf by guest on 21 August 2022

REFERENCES

Arnal, M., and Friedrich, R., 1991, "Large-Eddy Simulation of a Turbulent Flow with Separation," Turbulent Shear Flows 8, Springer-Verlag.

Avva, R., 1993, "CFD-ACE: Theory Manual," CFDRC Report GR-93-1.

Choudhury, D., and Kim, S., 1993, "Calculation of Turbulent Separated Flows Using a Renormalization Group Based k-ε Turbulence Model," Fluids Engineering Division, Vol. 149, Separated Flows, ASME.

Franke, R., and Rodi, W., 1991, "Calculation of Vortex Shedding Past a Square Cylinder with Various Turbulence Models," Turbulent Shear Flows 8, Springer-Verlag.

Geropp, D., and Leder A., 1985, "Turbulent Separated Flow Structures Behind Bodies with Various Shapes," International Conference on Laser Anemometry - Advances and Application, Manchester, UK.

Gould, R., 1994, "Analysis of Laser Doppler Velocimetry Data," Final Report for Summer Research Program, WL, AFOSR.

Gould, R., Stevenson W., and Thompson, D., 1988, "Turbulence Characteristics of an Axisymmetric Reacting Flow," NASA Contractor Report 4110.

Hosokawa, S., Ikeda, Y., Minato, M., and Nakajima, T., 1993, "Flow Measurements Behind V-Gutter Under Non-Combusting Condition," AIAA-93-0020.

Kim, J., Kline, S., and Johnston, J., 1978, "Investigation of Separation and Reattachment of a Turbulent Shear Layer: Flow Over a Backward-Facing Step," Report MD-37, Thermo Sciences Division, Dept. of Mechanical Engineering, Stanford University.

Kodali, V., and Amano, R., 1986, "Prediction of Turbulent Flows Behind Bluff Bodies by Using an Algebraic-Stress Model," AIAA-86-1061.

Larousse, A., Martinuzzi, R., and Tropea, C., 1991, "Flow Around Surface-Mounted, Three-Dimensional Obstacles," Turbulent Shear Flows 8, Springer-Verleg, pp.127-139.

Mansingh, V., and Oosthuizen, P., 1990, "Effects of Splitter Plates on the Wake Flow Behind a Bluff Body," AIAA Journal, pp. 778-783.

Martensson, H., Eriksson, L., and Albraten, P., 1991, "Numerical Simulations of Unsteady Wakeflow," 10th International Symposium on Air-Breathing Engines (ISABE), Vol. 2, Nottingham, England.

Pearce, J., Qasim, A., Maxwell, T., and Paramesawaran, S., 1992, "A Computational Study of Coherent Wake Structures Behind 2-D Bluff Bodies," J. of Wind Engineering and Industrial Aerodynamics, 41-44, pp. 2853-2861.

Perry, A., and Steiner, T., "Large-Scale Vortex Structures in Turbulent Wakes Behind Bluff Bodies: Part 1. Vortex Formation Processes," J. Fluid Mech., vol. 174, pp. 233-270.

Przulj, V., and Younis, B., 1993, "Some Aspects of the Prediction of Turbulent Vortex Shedding," Fluids Engineering Division, Vol. 149, Separated Flows, ASME.

Raffoul, C., Nejad, A., Spring, S., Kirkendall, C., and Smith, C., 1994, "Entrainment and Mixing Characteristics of Bluff Body Flameholders; an Experimental and Numerical Study," AIAA 94-0710.

Ryden, R., Eriksson, L., and Olovsson, S., 1993, "Large-Eddy Simulation of Bluff Body Stabilised Turbulent Premixed Flames," ASME 93-GT-157.

Sjunnesson, A., Olovsson, S., and Sjoblom, B., 1991, "Validation Rig - A Tool for Flame Studies," 10th International Symposium on Air Breathing Engines (ISABE), Nottingham, England.

Speziale, C., and Thangam, S. 1992, "Analysis of an RNG Based Turbulence Model for Separated Flows," NASA CR 189600.

Werner, H., and Wengle, H., 1991, "Large-Eddy Simulation of Turbulent Flow Over and Around a Cube in a Plate Channel," Turbulent Shear Flows 8, Springer-Verlag.

Yakhot, V., Orszag, S., 1986, "Renormalization Group Analysis of Turbulence. I. Basic Theory," J. Sci. Comput. **1**, 3.

Yakhot, V., Orszag, S., Thangan, S., Gatski, T., and Speziale, C., 1992, "Development of Turbulence Models for Shear Flows by a Double Expansion Technique," Phys. Fluids, A.4 (7).

Yang, K., and Ferziger, J., 1993, "Large-Eddy Simulation of Turbulent Obstacle Flow Using a Dynamic Subgrid-Scale Model," AIAA Journal, Vol. 31, No. 8.

Downloaded from http://asmedigitalcollection.asme.org/GT/proceedings-pdf/GT1995/78804/V003T06A016/2406276/v003t06a016-95-gt-102.pdf by guest on 21 August 2022